AIMS Mathematics, 10(12): 30229–30245.
DOI: 10.3934/math.20251328
Received: 06 October 2025
Revised: 26 November 2025
Accepted: 01 December 2025
Published: 24 December 2025

https://www.aimspress.com/journal/Math

*Research article*

# Investigating slip boundary in MHD Powell–Eyring fluid flow over a stretching sheet in porous domain with heat generation

**Fahad M. Alharbi***

Department of Mathematics, Al-Qunfudah University College, Umm Al-Qura University, Mecca, Saudi Arabia

* **Correspondence:** Email: fmsharbi@uqu.edu.sa.

**Abstract:** A steady, laminar, and incompressible flow of Powell–Eyring fluid model over a linearly stretching sheet is numerically investigated in a porous, two-dimensional medium. An influence of a slip velocity phenomenon, magnetic field, viscous dissipation, heat source, and radiation on the fluid flowing are considered with this investigation. The governing equations for this scenario are derived and then transformed to be dimensionless using a suitable similarity. The set of equations is solved numerically utilizing bvp4c built–in solver in MATLAB® software. To validate our results, a special case arising from this problem is obtained which shows a very good agreement with the previous studies. The effect of the considered physical quantities on the dimensionless velocity profile, temperature distribution, skin friction, and local Nusselt coefficient are described. Findings reveal that a resistance in the fluid flow and a growth in the thermal distribution have been noticed when the slip velocity phenomena, magnetic field, or permeability parameter is increased, whereas enhancing the velocity profile and thermal distribution can markedly be seen by increasing the radiation magnitude.

**Keywords:** Powell–Eyring fluid; MHD; slip velocity; porous medium; thermal radiation

## Nomenclature

| | |
|---|---|
| $a(s^{-1})$ and $T(K)$ | Stretching rate and temperature |
| $b(m\ s^2\ kg^{-1})$ and $c(s^{-1})$ | Fluid parameters |
| $B_0(A/m)$ | Constant magnetic field |
| $C_f$ | Skin friction coefficient |
| $C_p(J\ kg^{-1}\ K^{-1})$ | Specific heat at constant pressure |
| $f(m\ s^{-1})$ | Dimensionless velocity |

| | |
|---|---|
| $g(m\ s^{-2})$ | Acceleration due to gravity |
| $k(W\ m^{-1}\ K^{-1})$ | Thermal conductivity |
| $M$ and $R$ | Magnetic and thermal radiation coefficient |
| $Pr$, $Ec$, $Nu$ and $R_e$ | Prandtl, Eckert, Local Nusselt and Reynolds number |
| $Q$ | Dimensionless heat source coefficient |
| $Q_0(kg\ m^{-1}\ K^{-1}\ s^{-3})$ | Heat source |
| $q_w(W\ m^{-2})$ | Heat flux |
| $u$ and $v(m\ s^{-1})$ | Velocity components in $x-$, $y-$ axis |
| $x\ (m)$ and $y\ (m)$ | Cartesian coordinates |
| $\alpha$ and $\beta$ | Dimensionless radiation and convection coefficient |
| $\beta_0(K^{-1})$ and $\sigma(\Omega m^{-1})$ | Volumetric temperature and electrical conductivity |
| $\kappa(m^{-2})$ | Permeability of porous medium |
| $\kappa^*$ and $\sigma^*$ | Rosseland mean absorption and Stefan–Boltzman coefficient |
| $\lambda_1$ and $\lambda_2$ | Dimensionless fluid parameters |
| $\mu(N\ s\ m^{-2})$ | Dynamic viscosity |
| $\nu(m^2\ s^{-1})$ and $\rho(kg\ m^{-3})$ | Kinematic viscosity and density |
| $\psi_0(s\ m^{-1})$ and $\eta$ | Slip parameter and similarity variable |
| $K$ and $\psi$ | Dimensionless permeability and slip coefficient |

## 1. Introduction

A steady and an incompressible flow of the magnetohydrodynamics (MHD) Powell–Eyring fluid model in a porous medium has been considered over a linearly stretching sheet with the presence of the slip velocity. Such fluid is a non-Newtonian fluid that features a non-linear relationship between the shear stress and the rate of shearing [1]. Utilizing this model in the boundary layer region is of interest in industrial processes, material processing, biomedical applications, and many more [2]. MHD investigates the behavior of eclectically conducting fluids in a framework of an effect of magnetic fields. MHD flows provide significant features in numerous applications, including crystal growth, plasma, metal cooling, nuclear reactors, and more [3]. In addition, the boundary layer flow on a stretching sheet has found crucial significance in numerous engineering applications and manufacturing processes like plastic extrusion, metal rolling, glass fiber, and paper production [4, 5].

For the Newtonian fluid past a stretching sheet, the exact solution has been readily obtained by Crane [6]. Later, McLeod et al. [7] validated the solution of Crane [6] by presenting the uniqueness of the exact solution. Further pioneering investigations that incorporate nw innovations have been

produced, where the analytical solution is still achievable. For example, Gupta et al. [8] analyzed the fluid flow over a linearly stretching sheet subject to suction or blowing. The flow through a stretching channel was investigated by Brady et al. [9], while the flow over the stretching channel was analyzed by Wang [10]. Following a similar methodology but in three dimensions, Wang [11] obtained the analytical solution of the fluid flow arising from a stretching flat sheet. The unsteady boundary layer motion past a stretching surface has been investigated in various scenarios – see for example Wang [12] and Usha et al. [13].

However, for a non-Newtonian fluid, which is one of the most common materials used in industrial applications, the nonlinearity of the fluid equations makes the possibility of achieving the analytical solution more difficult except in very special cases, such as that of [14]. Consequently, a numerical investigation that employs the non-Newtonian fluid has been attempted by numerous researchers (for example, [15–17]) to gain a better understanding of the fluid flow behavior and to reach a distinguished mechanism of the heat transfer, especially with the influence of the heat generation [18], mixed convection [19], and thermal conductivity [20]. In detail, Sedki [21] has investigated the impact of thermal radiation on MHD non-Newtonian fluid flow over a permeable nonlinear stretching sheet, where the main and significant result shows that the thickness of the momentum and thermal boundary layer increase with increasing thermal radiation. In a similar context, Amar et al. [22] considered MHD heat and mass transfer non-Newtonian fluid flow in a two dimensional boundary layer in a porous medium. Their analysis shows significant influences of the radiation, heat, thermophoresis, and Brownian motion on the flow system along with the skin friction and local Nusselt number.

It is seen that a Powell–Eyring fluid flow over a stretching sheet is given attention in the literature. For example, Rao et al. [23] explored the influence of mixed convection on the MHD Powell–Eyring fluid flow and the thermal transfer over a stretching surface. Their analysis discovered that the mixed convection has a significant effect on both the velocity profile and temperature distribution. Furthermore, the Cattaneo–Christov heat flux with convective boundary condition was considered by Yusuf et al. [24] in order to investigate the incompressible flow of MHD Powell–Eyring nanofluid over an exponentially stretching sheet. They revealed that uplifting the fluid parameter increases the flow velocity and decreases the temperature.

For the same fluid model but on a porous stretching cylinder, Rikitu [25] observed that the overall thermal system is successfully managed by the porous medium. In addition, he found that the local Nusselt number accelerates with the increase of magnetic parameter. In the same context, Khader et al. [26] observed a reduction in the velocity distribution by increasing the slip velocity parameter. Moreover, their analysis emphasized that the temperature distribution increases corresponding to the increase of the heat generation parameter or thermal conductivity. In terms of the flow over the exponential shrinking sheet, Agrawal et al. [27] considered the thermal radiation and other physical quantities to investigate the MHD Powell–Eyring fluid flow. They observed that increasing the thermal radiation improves the velocity and temperature profile. The variation of the MHD Powell–Eyring fluid flow due to the impact of the permeability, heat source, radiation, and magnetic parameter, over the linearly elongated surface has been explored by Karthik et al. [28]. The outcomes emphasized the deceleration of the velocity profile as the porous parameter increases. Furthermore, the impact of multiple slip velocities along with other physically interesting parameters on the Powell–Eyring nanofluid past porous stretching surface have been investigated by Patil et al. [29]. It

is asserted that the application of the magnetic field provides a remarkable effect by displaying a decline in the velocity profile and an increase in both thermal and solutal boundary layers. Their calculation excludes the viscous dissipation effect on the velocity profile and the thermal distribution.

In instruments that deal with high temperature, such as nuclear power plants, the influence of radiation on modeling MHD flow is always of interest. Srivastava et al. [30] analyzed the influence of the buoyancy and thermal radiation on a MHD free-convection boundary layer across a stretchable porous sheet. Considering an exponentially stretched permeable sheet in porous medium, the mixed convection MHD flow associated with the physical quantities such as the impact of magnetic field, Prandtl number, viscosity, and conductivity, is numerically analyzed by Knowar et al [31]. Their analysis showed that the skin friction grows in response to the increase of mixed convection parameter and magnetic field, while the temperature wall increases due to enhancing the Prandtl number. Moreover, the effect factors arising from the viscous dissipation, the slip velocity, and Joule heating were considered in the investigation of Abbas et al. [32]. Their finding displays that the nanofluid thermal temperature is increased by enhancing magnetic field and viscous dissipation, whereas the slip velocity provides an opposite impact. However, the influence of the porous medium and volumetric temperature coefficient on the flow field were omitted in their analysis. Note that although the significance of the magnetic field influence on heat and mass transfer has been shown recently, there are markedly limited investigations for its effect in cases involving a slip velocity phenomenon, porous medium, and viscous dissipation, among others physical quantities.

In this analysis, we numerically investigate MHD flow of the Powell–Eyring fluid and thermal transfer over a linearly stretching surface in a porous medium. In addition, the effects of the slip velocity phenomena, viscous dissipation, heat source, and radiation are taken into account. The governing equations for this investigation are derived and then transformed to be dimensionless using a suitable similarity. The set of equations is solved numerically utilizing a bvp4c built–in solver in MATLAB® software. In order to validate our investigation, the particular case arising from the current problem will be obtained and compared with those in the literature. The comparison between the results will show a strong agreement. The outcomes of such analysis will provide a comprehensive information about the variation of the fluid velocity profile as well as the thermal distribution resulting from the unsteadiness of the considered physical parameters. Finally, the numerical data of the skin friction coefficient along with the local Nusselt number will be provided in a table for appropriate values of the physical parameters. Note that the application of thermal radiation in magnetic hydrodynamic fluid flow plays a major role in monitoring heat relocation, arising from both the magnetic field and heat source, in the polymer preparation industry, whereas the convection coefficient quantifies the heat transfer rates throughout the boundary layer field.

## 2. Governing equations

A steady, laminar, and incompressible flow of an Eyring–Powell fluid model past a linearly elongated sheet in a porous medium of permeability $\kappa$ is considered in two–dimensions, where the $x$–axis is taken along the surface, while the $y$–axis is perpendicular to it. Such flow is generated by continuously extending the surface with a linear velocity $U = ax$, where $a$ is the enlarging rate of the sheet, and the slip velocity is applied to the fluid. The fluid temperature at the surface and the free stream are defined by $T_w$ and $T_\infty$, respectively. In addition, it is assumed that the energy equation will

be involved with the heat source, viscous dissipation, and radiation. The physical problem together with the coordinate system are shown in Figure 1.

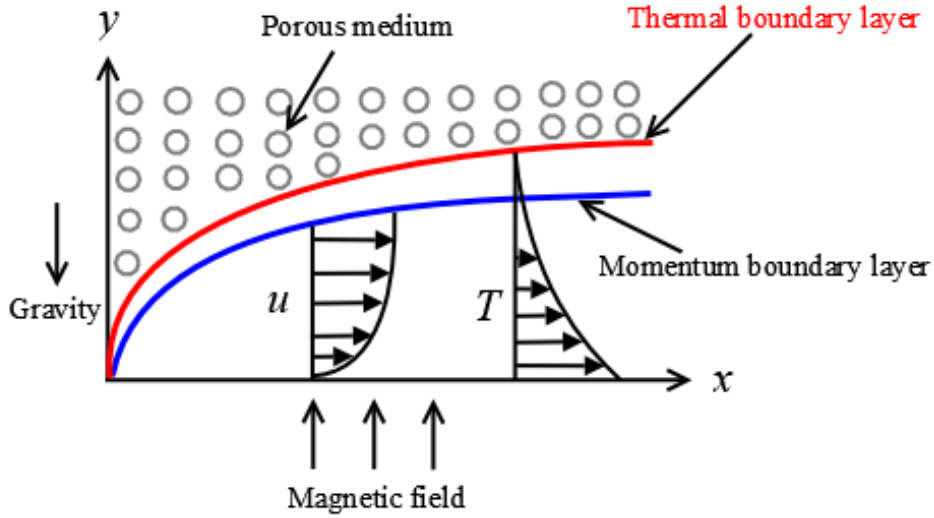


**Figure 1.** A schematic diagram illustrates the physical problem in Cartesian coordinates.

Considering the above, the continuity and momentum equations for the Powell–Eyring fluid model are given by [2, 33]:

$$\frac{\partial u}{\partial x} + \frac{\partial v}{\partial y} = 0, \tag{2.1}$$

$$\begin{aligned} u\frac{\partial u}{\partial x} + v\frac{\partial v}{\partial y} = \left(\nu + \frac{1}{\rho bc}\right)\frac{\partial^2 u}{\partial y^2} - \frac{1}{2bc^3\rho}\left(\frac{\partial u}{\partial y}\right)^2\frac{\partial^2 u}{\partial y^2} + \\ g\beta_0\left(T - T_\infty\right) - \left(\frac{\sigma B_0^2}{\rho} + \frac{\nu}{\kappa}\right)u, \end{aligned} \tag{2.2}$$

and the energy equation with the presence of heat source, viscous dissipation, and radiation yields [34]

$$u\frac{\partial T}{\partial x} + v\frac{\partial T}{\partial y} = \frac{k}{\rho C_p}\frac{\partial^2 T}{\partial y^2} - \frac{1}{\rho C_p}\frac{\partial q_r}{\partial y} + \frac{\mu}{\rho C_p}\left(\frac{\partial u}{\partial y}\right)^2 + \frac{Q_0}{\rho C_p}\left(T - T_\infty\right), \tag{2.3}$$

where $u$ and $v$ represent the velocity components along the $x$ and $y$ axis, respectively. In addition, $\nu$ and $\rho$ are the kinematic viscosity and density, respectively. Moreover, $b$ and $c$ are the fluid parameters. Furthermore, $g, \beta_0, \sigma$, and $B_0$ are the acceleration due to gravity, volumetric temperature coefficient, the electrical conductivity of the fluid, and the strength of the magnetic field, respectively. It is assumed that the constant and homogeneous magnetic field $B_0$ is applied in the transverse of the surface, while the induced magnetic field, which is applied perpendicular to $B_0$, is neglected due to its

weak intensity compared to the $B_0$ field. $T$ is the fluid temperature, whereas $k, C_p, \mu$, and $Q_0$ are the thermal conductivity, the specific heat, dynamic viscosity, and heat source, respectively.

Note that the second term in the right side of (2.3) regards the radiative heat flow, which is assumed to take the following form [35, 36]:

$$q_r = -\frac{4\sigma^*}{3k^*}\frac{\partial T^4}{\partial y}, \tag{2.4}$$

where $k^*$ and $\sigma^*$ are the Rosseland mean absorption and the Stefan–Boltzman coefficient, respectively. In this paper, we assume that the variation of the temperature within the flow is sufficiently small. Thus, we may express $T^4$ as a linear function of temperature. Accordingly, expanding $T^4$ in a Taylor series about $T_\infty$ along with neglecting higher order terms yields

$$T^4 \cong 4T_\infty^3 T - 3T_\infty^4. \tag{2.5}$$

Substituting (2.5) in (2.4), we reach

$$\frac{\partial q_r}{\partial y} = -\frac{16\sigma^* T_\infty^3}{3k^*}\frac{\partial^2 T}{\partial y^2}. \tag{2.6}$$

Substituting (2.6) in (2.3) yields

$$u\frac{\partial T}{\partial x} + v\frac{\partial T}{\partial y} = \frac{k}{\rho C_p}\frac{\partial^2 T}{\partial y^2} + \frac{16\sigma^* T_\infty^3}{3k^*\rho C_p}\frac{\partial^2 T}{\partial y^2} + \frac{\mu}{\rho C_p}\left(\frac{\partial u}{\partial y}\right)^2 + \frac{Q_0}{\rho C_p}\left(T - T_\infty\right). \tag{2.7}$$

From (2.7), the last term in the right side, $Q_0\left(T - T_\infty\right)$, is the heat source that measures the rate of heat transfer between the fluid particles and its surroundings, where $Q_0$ is the constant that represents a baseline of the heat quantity. Setting $T = T_w$, where $T_w$ is the temperature of the surface, we reach a constant term that describes the temperature difference between a surface and the surrounding fluid.

The relative boundary conditions of our problem are introduced by

$$\begin{aligned} &u(x,0) = ax + \psi_0\nu\left(\left(1 + \frac{1}{\mu bc}\right)\frac{\partial u}{\partial y} - \frac{1}{6\mu bc^3}\left(\frac{\partial u}{\partial y}\right)^3\right),\\ &v(x,0) = 0,\ T(x,0) = T_w,\\ &u(x,\infty) = v(x,\infty) = 0, \quad T(x,\infty) = T_\infty, \end{aligned} \tag{2.8}$$

where $\psi_0$ is the slip parameter.

In what follows, we render dimensionless the constitutive equations along with the boundary conditions, given in (2.1–2.2) and (2.7–2.8), using the following new variables [37]:

$$\begin{aligned} &\eta = \sqrt{\frac{a}{\nu}}y, \quad u = axf'(\eta), \quad v = -\sqrt{a\nu}f(\eta),\\ &T = (T_w - T_\infty)\theta(\eta) + T_\infty, \end{aligned} \tag{2.9}$$

where $\eta$ is a dimensionless constraint, and the continuity equation (2.1) is met.

Applying (2.9) in (2.1–2.2) and (2.7–2.8) yields

$$\left((1+\lambda_1)-\lambda_1\lambda_2 f''^2\right) f''' + f f'' + \beta\theta - (K+M+f')\, f' = 0, \tag{2.10}$$

$$\alpha\theta'' + Pr\left(f\theta' + Ec f''^2\right) + Q\theta = 0, \tag{2.11}$$

subject to the boundary conditions

$$\begin{aligned} &f(0) = 0, \quad f'(0) = 1 + \psi\left((1+\lambda_1)\, f''(0) - \frac{\lambda_1\lambda_2}{3} f''^3(0)\right), \quad \theta(0) = 1, \\ &f'(\infty) = 0, \quad \theta(\infty) = 0, \end{aligned} \tag{2.12}$$

where the prime denotes the derivative with respect to $\eta$. In addition, $\lambda_1 = \frac{1}{\rho v b c}$ and $\lambda_2 = \frac{aU^2}{2vc^2}$ are the fluid parameters; $\beta = \frac{g\beta_0(T_w - T_\infty)}{aU}$ is the convection parameter; $K = \frac{\nu}{\kappa a}$ is the permeability coefficient; $M = \frac{\sigma\beta_0^2}{\rho a}$ is the magnetic coefficient; $\alpha = 1 + \frac{4}{3}R$, where $R = \frac{4\sigma^* T_\infty^3}{kk^*}$ is the Radiation coefficient; $Pr = \frac{\rho C_p \nu}{k}$ is the Prandtl number; $Ec = \frac{U^2}{C_p(T_w - T_\infty)}$ is the Eckert number; $Q = \frac{Q_0 \nu}{ak}$ is the heat source coefficient; and $\psi = \psi_0\sqrt{a\nu}$ is the slip coefficient.

The quantities of practical interest for this mathematical modeling are the skin friction coefficient, $C_f$, and local Nusselt number, $Nu$, where their formulations take the following form [2]:

$$C_f = \frac{\tau_w}{\rho a^2 x^2}, \quad Nu = \frac{x q_w}{k(T_w - T_\infty)}, \tag{2.13}$$

and the shear stress, $\tau_w$, as well as the heat flux, $q_w$, are given by

$$\tau_w = \left(\mu + \frac{1}{bc}\right)\frac{\partial u}{\partial y} - \frac{1}{6bc^3}\left(\frac{\partial u}{\partial y}\right)^3\Bigg|_{y=0}, \quad q_w = -k\frac{\partial T}{\partial y} + q_r\Bigg|_{y=0}. \tag{2.14}$$

Applying (2.9) in the first and the second of (2.13) yields, on considering (2.14),

$$\sqrt{Re}C_f = (1+\lambda_1) f''(0) - \frac{\lambda_1\lambda_2}{3} f''^3(0), \quad \frac{Nu}{\sqrt{Re}} = -(1+4R)\theta'(0), \tag{2.15}$$

presenting the skin friction coefficient and the local Nusselt number in dimensionless form, where $Re = \frac{ax^2}{\nu}$ is the local Reynolds number.

## 3. Numerical method

The similarity transformation (2.9) successfully converts our system to nonlinear ordinary differential equations. The unknown quantities in the problem (2.10)–(2.12) are the integration constants for the functions $f(\eta)$ and $\theta(\eta)$, whereas the rest of the parameters are assumed known. Note that due to the presence of the nonlinearity in the system, the exact solution is far from achieved, so the numerical technique must be adapted. Thus, the *bvp4c* built–in solver in MATLAB® software is utilized in order to transfer the boundary value problem to an initial value one. Then, the initial guesses are selected to satisfy the boundary conditions. A convergence criterion is of the order $10^{-6}$ for the gained results. The flow chart, given in Figure 2, describes such numerical computation.

Therefore, the transformation of our system to an initial value problem (IVP) is as follows:

$$\begin{aligned} &y_1 = f, \quad y_2 = f', \quad y_3 = f'', \quad y_3' = f''' \\ &y_4 = \theta, \quad y_5 = \theta', \quad y_5' = \theta''. \end{aligned} \tag{3.1}$$

In programming, the new set of variables takes the form

$$y_1' = y_2, \tag{3.2}$$
$$y_2' = y_3, \tag{3.3}$$
$$y_3' = \frac{1}{\left((1+\lambda_1) - \lambda_1\lambda_2 y_3^2\right)} \left((K + M + y_2)y_2 - y_1 y_3 - \beta y_4\right), \tag{3.4}$$
$$y_4' = y_5, \tag{3.5}$$
$$y_5' = -\frac{Pr}{\alpha}\left(y_1 y_5 + Ec y_3^2\right) - \frac{Q}{\alpha} y_4, \tag{3.6}$$

while the boundary conditions become

$$\begin{aligned} &y_1 = 0, \quad y_2 = 1 + \psi\left((1+\lambda_1)y_3 - \frac{\lambda_1\lambda_2}{3} y_3^3\right), \quad y_4 = 1, \quad \text{at} \quad \eta = 0, \\ &y_2 \to 0, \quad y_4 \to 0, \quad \text{as}, \quad \eta \to \infty, \end{aligned} \tag{3.7}$$

whereas the skin friction and Nusselt number convert to

$$\sqrt{Re} C_f = (1+\lambda_1)y_3(0) - \frac{\lambda_1\lambda_2}{3} y_3^3(0), \tag{3.8}$$
$$\frac{Nu}{\sqrt{Re}} = -(1+4R)y_5(0). \tag{3.9}$$

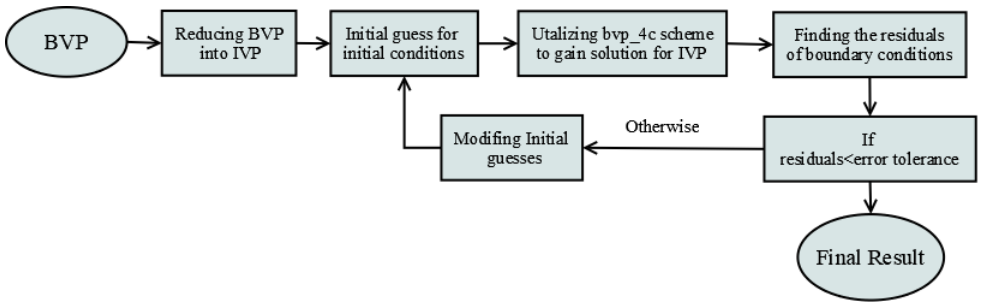


**Figure 2.** The flow chart of the numerical computation of the boundary value problem.

To validate this technique, the maximum residual and mesh points are presented in Table 1. It can clearly be seen that the maximum error is approximately $9.5 \times 10^{-7}$, which indicates a very good accuracy for the numerical results. In addition, the current results are compared with those in the literature in Table 2 and show a strong accuracy.

**Table 1.** The numerical data that describe the maximum residual and mesh points of the velocity profile, $f'(\eta)$, where $\eta = [0 : 10 : 8]$, $\lambda_1 = 0.1, \lambda_2 = 0.3, \beta = 0.2, Q = 0.3$, and $Ec = 0.1$.

| $\psi$ | $R$ | $K$ | $Pr$ | $M$ | Maximum Residual | Mesh Points |
|---|---|---|---|---|---|---|
| 0 | 1 | 0.5 | 3 | 2 | $9.5 \times 10^{-7}$ | 92 |
| 0.3 | | | | | $9.8 \times 10^{-7}$ | 85 |
| 0.9 | | | | | $9.5 \times 10^{-7}$ | 65 |
| 0.3 | 3 | | | | $9.5 \times 10^{-7}$ | 92 |
| | 5 | | | | $9.8 \times 10^{-7}$ | 85 |
| | 1 | 1 | | | $9.4 \times 10^{-7}$ | 65 |
| | | 1.5 | | | $9.7 \times 10^{-7}$ | 85 |
| | | 0.5 | 5 | | $9.2 \times 10^{-7}$ | 87 |
| | | | 7 | | $9.5 \times 10^{-7}$ | 85 |
| | | | 3 | 4 | $9.8 \times 10^{-7}$ | 85 |
| | | | | 6 | $9.2 \times 10^{-7}$ | 87 |

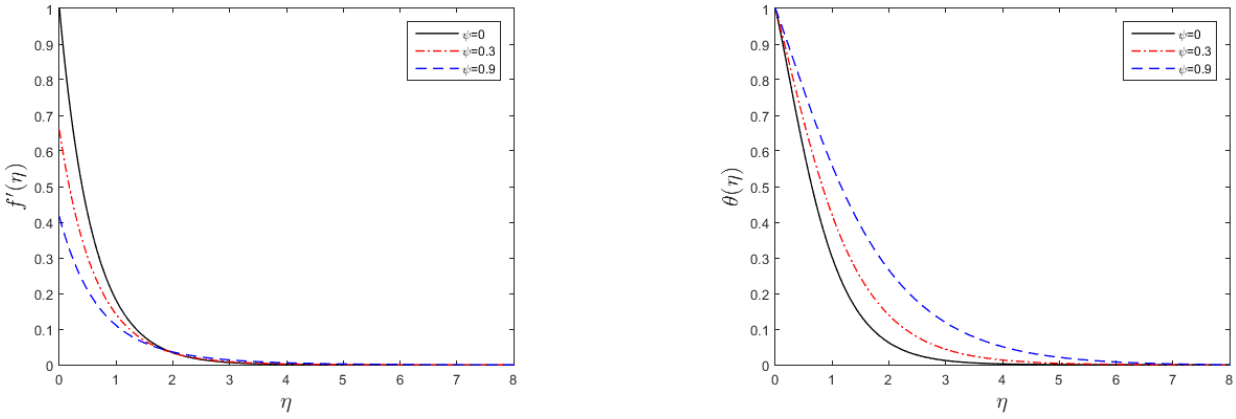


**(a)** **(b)**

**Figure 3.** The variation of the velocity profile (**a**) and the temperature distribution (**b**) for numerous values of the slip parameter, $\psi$, where $\lambda_1 = 0.1, \lambda_2 = 0.3, Q = 0.3, Ec = 0.1, R = 1, K = 0.5, Pr = 7, M = 2$, and $\beta = 0.2$.

## 4. Result and discussion

In this section, we demonstrate the influence of numerous physical constraints on the Powell–Eyring fluid flow and heat transfer over a steady stretching surface. In particular, the effect of the slip velocity $\psi$, the magnetic field $M$, the convection $\beta$, the Prandtl number $Pr$, the radiation $R$, and the permeability parameter $K$ are discussed. Thus, the dimensionless velocity, $f'(\eta)$, and the temperature, $\theta(\eta)$, fields have been generated in Figures 3a and 3b, respectively, for various values of $\psi$. It is seen that increasing the magnitude of the slip parameter leads to decreasing the fluid velocity and increasing the temperature profile. Physically, such slip phenomena may be attributed to reflect the presence of roughness on the

stretching sheet.

Figure 4 demonstrates the effect of the magnetic field on the velocity and heat profile. In Figure 4a, it is clear that the fluid flow decelerates as the magnetic parameter value increases, whereas Figure 4b displays a remarkable increase in the temperature magnitude by enhancing the magnetic parameter. Physically, the presence of the magnetic field would create a resistive force acting on the fluid particles, slowing the velocity field of the fluid. Thus, such fluid particles gain some heat energy from the same applied force.

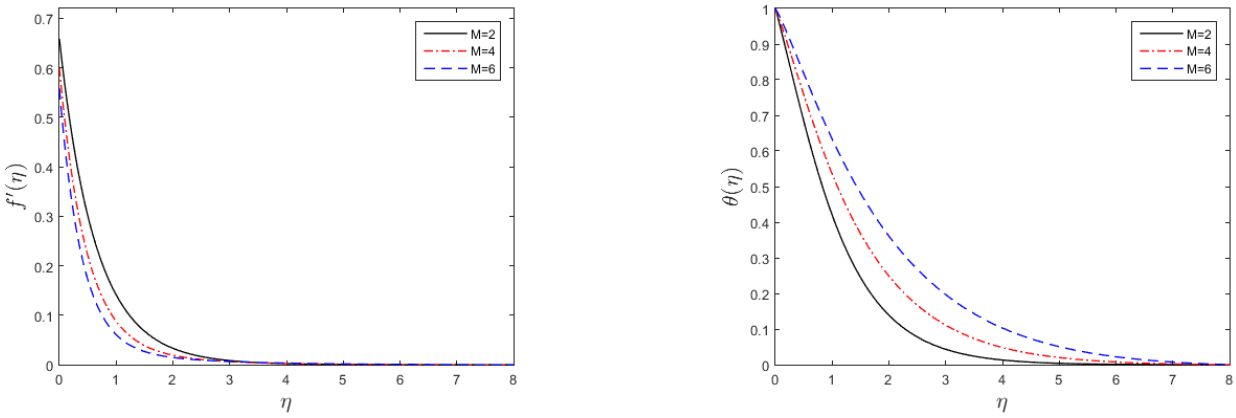


**(a)** **(b)**

**Figure 4.** The variation of the velocity profile (**a**) and the temperature distribution (**b**) for numerous values of the magnetic parameter, $M$, where $\lambda_1 = 0.1, \lambda_2 = 0.3, Q = 0.3, Ec = 0.1, R = 1, K = 0.5, Pr = 7, \psi = 0.3$, and $\beta = 0.2$.

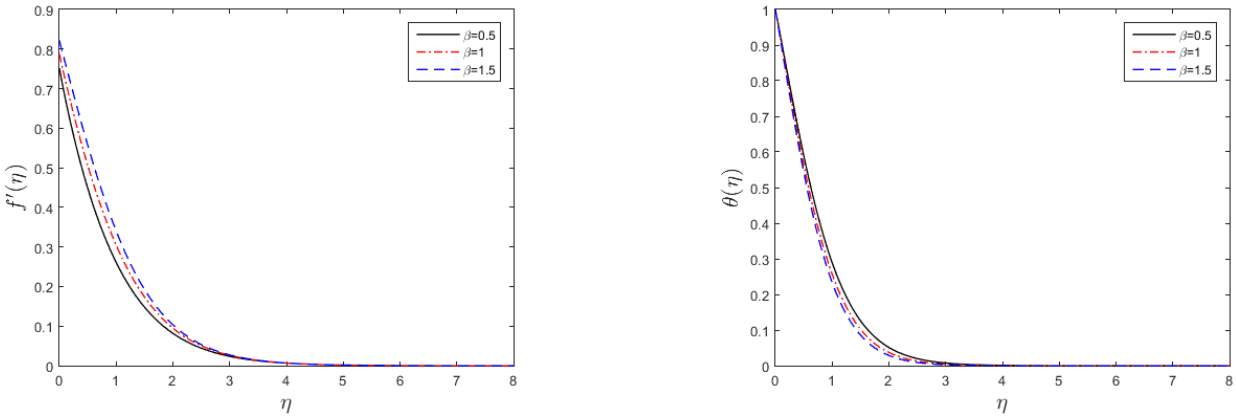


**(a)** **(b)**

**Figure 5.** The variation of the velocity profile (**a**) and the temperature distribution (**b**) for numerous values of the convection parameter, $\beta$, where $\lambda_1 = 0.1, \lambda_2 = 0.3, Q = 0.3, Ec = 0.1, R = 1, K = 0.5, Pr = 7, M = 2$, and $\psi = 0.3$.

Enhancing the mixed convection parameter $\beta$, the velocity overshoot is observed near the wall, as seen in Figure 5a. Accordingly, the velocity profile is noticeably increased within the boundary layer

field. Physically, increasing $\beta$ leads to heating of the fluid or cooling of the wall surface, which causes an increase in the fluid flow. On the other hand, in Figure 5b, it can be seen that when the $\beta$ value is increased, the thickness magnitude of thermal boundary layer becomes thinner, which in turn produces an increment in the magnitude of the wall temperature gradient, and hence the surface heat transfer rate is increased. This observation is in the parallel line to that in [38, 39].

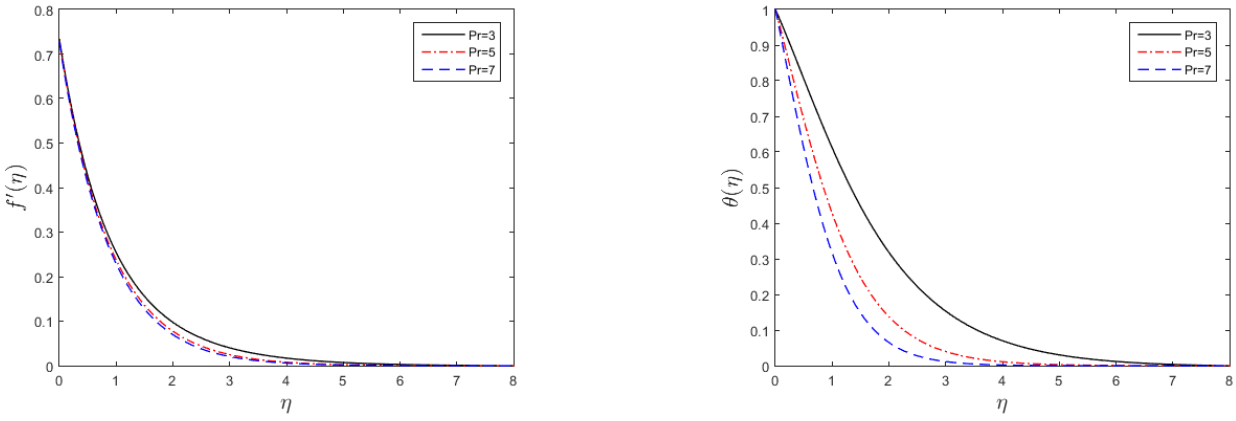


**(a)** **(b)**

**Figure 6.** The variation of the velocity profile (**a**) and the temperature distribution (**b**) for numerous values of the Prandtl number, $Pr$, where $\lambda_1 = 0.1, \lambda_2 = 0.3, Q = 0.3, Ec = 0.1, R = 1, K = 0.5, \psi = 0.3, M = 2$, and $\beta = 0.2$.

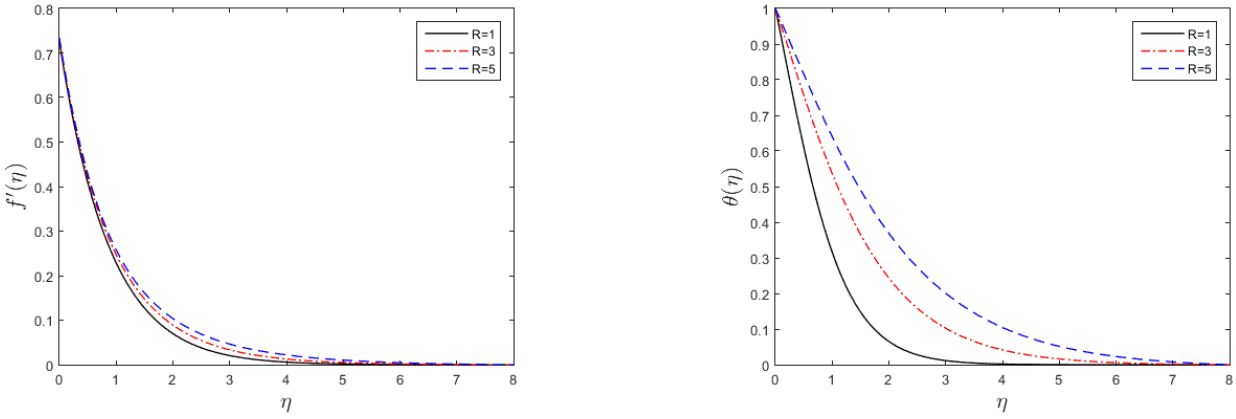


**(a)** **(b)**

**Figure 7.** The variation of the velocity profile (**a**) and the temperature distribution (**b**) for numerous values of the Radiation parameter, $R$, where $\lambda_1 = 0.1, \lambda_2 = 0.3, Q = 0.3, Ec = 0.1, \psi = 0.3, K = 0.5, Pr = 7, M = 2$, and $\beta = 0.2$.

The information about the effect of the Prandtl number, $Pr$, on the fluid flow field can be seen in Figure 6.

Clearly, we observe that when $Pr$ is increased, the velocity (in Figure 6a) and the temperature (in Figure 6b) profile decline over the sheet. Such behavior occurs due to the fact that upon enhancing the

Prandtl number, the fluid becomes more viscous, which leads to the deceleration of the fluid velocity and temperature distribution.

Figures 7a and 7b elucidate the influence of the radiation parameter $R$ on the profile of the velocity and temperature. So, it can be deduced that both $f'(\eta)$ and $\theta(\eta)$ are increased with increasing $R$. This is analogous to what can be predicted from physical grounds, where increasing the thermal radiation leads to increasing the momentum of the fluid and hence increasing the velocity profile. Thus, such additional thermal radiation provides an extra heat energy to the heat transfer through the boundary layer, making the temperature thickness increase markedly.

The variation of the permeability parameter $K$ and its effect on the flow and thermal distribution is shown in Figures 8a and 8b, respectively. We can observe that increasing $K$ causes a reduction in the velocity profile. However, the temperature profile increases with increasing $K$. The physical interpretations of such behavior indicate that enhancing the permeability parameter produces a resistance that loses the momentum of the fluid and hence reduces the fluid velocity. Because the velocity field dampens because of the increased permeability, the fluid particles take much time in any region, especially closing to the stretching sheet, which makes the fluid particles receive more heat energy, increasing the temperature throughout the boundary layer.

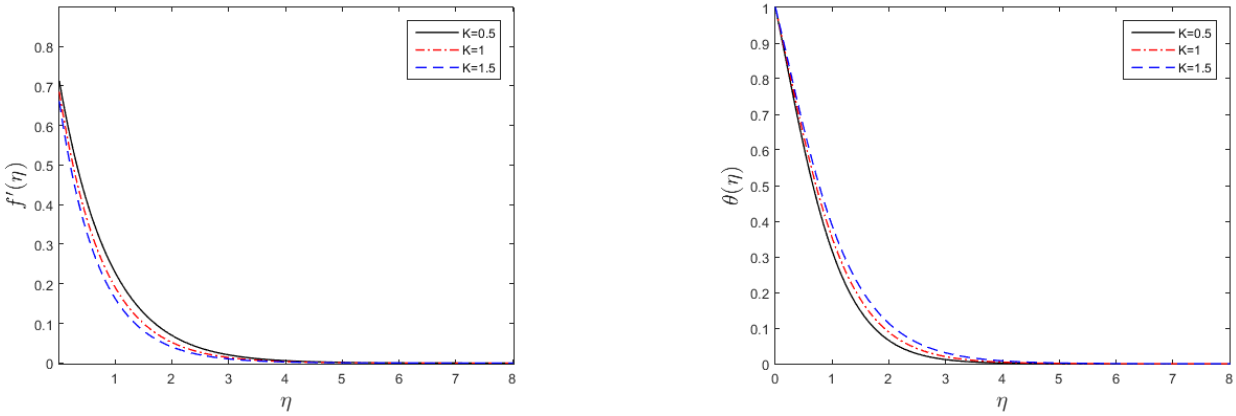


**(a)** **(b)**

**Figure 8.** The variation of the velocity profile (**a**) and the temperature distribution (**b**) for numerous values of the permeability parameter, $K$, where $\lambda_1 = 0.1, \lambda_2 = 0.3, Q = 0.3, Ec = 0.1, R = 1, \psi = 0.3, Pr = 7, M = 2$, and $\beta = 0.2$.

Setting the fluid parameters $\lambda_1 = \lambda_2 = 0$, the permeability parameter $K = 0$ and the convection parameter $\beta = 0$ along with the absence of the slip parameter $\psi = 0$, our problem reduces to those considered in [37, 40]. Thus, to validate our numerical scheme, Table 2 compares the current friction coefficient values $C_f \sqrt{Re}$ with those presented in [37, 40] for various values of the magnetic parameter $M$. This shows a very good agreement between the results.

**Table 2.** Comparison between the current results with those of [37] and [40] for skin friction coefficient, $C_f\sqrt{Re}$, where $\lambda_1 = \lambda_2 = K = \beta = \psi = 0$.

| $M$ | Current results | Akbar et al [37] | Fathizadeh et al [40] |
|---|---|---|---|
| 0 | −1 | −1 | −1 |
| 1 | −1.41421 | −1.41421 | −1.41421 |
| 5 | −2.44951 | −2.44949 | −2.44948 |
| 10 | −3.31661 | −3.31663 | −3.31662 |
| 100 | −10.04988 | −10.04988 | −10.04988 |
| 500 | −22.38301 | −22.38303 | −22.38302 |
| 1000 | −31.63859 | −31.63859 | −31.63858 |

The numerical results, which are generated in Table 3, demonstrate the influence of $\psi, R, K, Pr$, and $M$ on the fractional drag or the skin fractional coefficient, $C_f\sqrt{Re}$, and the heat transfer rate of the Nusselt number, $Nu/\sqrt{Re}$. It is observed that increasing the slip parameter, $\psi$, leads to decreasing both $C_f\sqrt{Re}$ and $Nu/\sqrt{Re}$, where $\lambda_1 = 0.1, \lambda_2 = 0.3, Ec = 0.1$, $Q = 0.3$, and $\beta = 0.2$ are held fixed. Moreover, escalating the radiation parameter, $R$, decelerates $C_f\sqrt{Re}$ and accelerates $Nu/\sqrt{Re}$ and vice versa for the permeability parameter, $K$. For the Prandtl number, $Pr$, it is shown that $C_f\sqrt{Re}$ and $Nu/\sqrt{Re}$ increase with increasing $Pr$. The significant change in $C_f\sqrt{Re}$ and $Nu/\sqrt{Re}$ values is seen with the variation of the magnetic parameter, $M$, where $C_f\sqrt{Re}$ is increased, while $Nu/\sqrt{Re}$ is declined as $M$ increases.

**Table 3.** variation of the skin friction coefficient, $C_f\sqrt{Re}$, and the Nusselt number, $Nu/\sqrt{Re}$, at the different appropriate values of particular selected constraints, where $\lambda_1 = 0.1, \lambda_2 = 0.3, \beta = 0.2, Q = 0.3$, and $Ec = 0.1$.

| $\psi$ | $R$ | $K$ | $Pr$ | $M$ | $C_f\sqrt{Re}$ | $Nu/\sqrt{Re}$ |
|---|---|---|---|---|---|---|
| 0 | 1 | 0.5 | 3 | 2 | −1.8563 | 1.5429 |
| 0.3 | | | | | −1.1283 | 1.0794 |
| 0.9 | | | | | −0.6431 | 0.6079 |
| 0.3 | 3 | | | | −1.1249 | 2.1668 |
| | 5 | | | | −1.1241 | 3.3985 |
| | 1 | 1 | | | −1.1873 | 0.8907 |
| | | 1.5 | | | −1.2399 | 0.7256 |
| | | 0.5 | 5 | | −1.1362 | 2.1555 |
| | | | 7 | | −1.1416 | 2.9924 |
| | | | 3 | 4 | −1.3306 | 0.4514 |
| | | | | 6 | −1.4720 | 0.0591 |

## 5. Conclusions

In this paper, we have successfully investigated the problem that involves flow and thermal transfer for Powell–Eyring fluid over a linearly stretching sheet with slip velocity phenomena. In addition, the

impact of a porous medium, viscous dissipation, heat source, and radiation are considered as well. Due to the complicated constraint equations, the appropriate dimensionless transformations are applied in order to convert the nonlinear partial differential equations into nonlinear ordinary ones. Such transformed equations are numerically solved subjects to the dimensionless boundary conditions. To validate the obtained results, a particular case from this investigation is obtained and compared with those obtained in the literature. The results of the present investigation can be addressed as follows:

- Enhancing the slip velocity leads to increasing the thermal distribution and decreasing the velocity profile, skin friction, and Nusselt number.
- Escalating the magnetic field declines the velocity profile, skin friction, and Nusselt number while enhancing the thermal distribution.
- Increasing the radiation effect increases the velocity profile, thermal distribution, and Nusselt number and declines the skin friction.
- Uplifting the permeability reduces the velocity profile and Nusselt number and increases the thermal distribution and skin fiction.
- Enlarging the Prandtl number decreases the velocity profile and thermal distribution and increases the skin friction and Nusselt number.

The advantages of the outcome results are to optimize the industrial processes and applications involving non-Newtonian fluids, particularly Powell–Eyring fluid.

## 6. Future work

The analysis of this paper might be extended by assuming MHD flow in an optically thick medium, arising from a shear-thickening fluid. As a result, the radiation energy might be absorbed and re-emitted many times within a short distance and hence the energy transfer may behave similarly to conduction. Therefore, the radiation approximation of (2.6) using the Taylor series around $T_\infty$ might not be available, and the diffusion approximation may be recommended. In addition, our problem could be investigated in other geometrical configurations like a flow field around a sphere.

## Use of Generative-AI tools declaration

The author declares that he has not used Artificial Intelligence (AI) tools in the creation of this article.

## Conflict of interest

The author declares that he has no conflicts of interest.

## References

1. C. Duan, M. Alhazmi, Z. Shah, M. Jawaid, M. E. Dalam, M. M. Almazah, et al., Numerical analysis of heat and mass transfer in eyring-powell fluid employing python with convective boundary conditions, *Case Stud. Therm. Eng.*, **73** (2025), 106546.

2. S. Karthik, D. Iranian, I. Khan, D. B. Basha, F. Hajjej, A. Singh, Heat transfer rate and thermal energy analysis of mhd powell-eyring fluid in a permeable medium, *Case Stud. Therm. Eng.*, **52** (2023), 103702.
3. Y. Vinod, K. Raghunatha, S. N. Nagappanavar, N. Nazarova, M. Gupta, et al., Boundary layer flow of a non-newtonian fluid over an exponentially stretching sheet with the presence of a heat source/sink, *Partial Differ. Eq. Appl. Math.*, **13** (2025), 101111.
4. K. Sudarmozhi, D. Iranian, N. Alessa, Investigation of melting heat effect on fluid flow with brownian motion/thermophoresis effects in the occurrence of energy on a stretching sheet, *Alex. Eng. J.*, **94** (2024), 366–376. http://doi.org/10.1016/j.aej.2024.03.065
5. J. Raza, F. Mebarek-Oudina, H. Ali, I. Sarris, Slip effects on casson nanofluid over a stretching sheet with activation energy: Rsm analysis, *Front. Heat Mass Transfer*, **22** (2024), 1017–1041.
6. L. J. Crane, Flow past a stretching plate, *ZAMP*, **21** (1970), 645–647. http://doi.org/10.1007/BF01587695
7. J. McLeod, K. Rajagopal, On the uniqueness of flow of a Navier–Stokes fluid due to a stretching boundary, *Arch. Ration. Mech. Anal.*, **98** (1987), 385–393.
8. P. Gupta, A. Gupta, Heat and mass transfer on a stretching sheet with suction or blowing, *Can. J. Chem. Eng.*, **55** (1977), 744–746.
9. J. Brady, A. Acrivos, Steady flow in a channel or tube with an accelerating surface velocity. An exact solution to the Navier–Stokes equations with reverse flow, *J. Fluid Mech.*, **112** (1981), 127–150. http://doi.org/10.1017/S0022112081000323
10. C. Y. Wang, Fluid flow due to a stretching cylinder, *Phys. Fluids*, **31** (1988), 466–468. http://doi.org/10.1063/1.866827
11. C. Wang, The three-dimensional flow due to a stretching flat surface, *Phys. Fluids*, **27** (1984), 1915–1917. http://doi.org/10.1063/1.864868
12. C. Wang, Liquid film on an unsteady stretching surface, *Q. Appl. Math.* , **48** (1990), 601–610. http://doi.org/10.1090/qam/1079908
13. R. Usha, R. Sridharan, The axisymmetric motion of a liquid film on an unsteady stretching surface, *J. Fluids Eng.*, **177** (1995), 81–85.
14. S. R. Munjam, K. Gangadhar, R. Seshadri, M. Rajeswar, Novel technique MDDIM solutions of MHD flow and radiative Prandtl–Eyring fluid over a stretching sheet with convective heating, *Int. J. Ambient Energy*, **43** (2022), 4850–4859.
15. W. Abbas, A. M. Megahed, M. Emam, H. M. Sadek, Mhd dissipative powell-eyring fluid flow due to a stretching sheet with convective boundary conditions and slip velocity, *Sci. Rep.*, **13** (2023), 15674.
16. S. Karthik, D. Iranian, Q. M. Al-Mdallal, Numerical simulation of magneto-hydrodynamic fluid flow with heat sink, chemical diffusion and powell eyring fluid behavior using cattaneo–christov source term, *Int. J. Thermofluids*, **22** (2024), 100616.
17. P. Agarwal, R. Jain, K. Loganathan, Thermally radiative flow of mhd powell-eyring nanofluid over an exponential stretching sheet with swimming microorganisms and viscous dissipation: A numerical computation, *Int. J. Thermofluids*, **23** (2024), 100773.

18. S. Sagheer, R. Razzaq, U. Farooq, Non-similar analysis of heat generation and thermal radiation on eyring-powell hybrid nanofluid flow across a stretching surface, *Adv. Mech. Eng.*, **16** (2024), 16878132241282562 .
19. B. Ahmed, T. Hayat, F. Abbasi, A. Alsaedi, Mixed convection and thermal radiation effect on mhd peristaltic motion of powell-eyring nanofluid, *Int. Commun. Heat Mass Transfer*, **126** (2021), 105320. http://doi.org/10.1016/j.icheatmasstransfer.2021.105320
20. A. S. Oke, W. N. Mutuku, Significance of viscous dissipation on mhd eyring–powell flow past a convectively heated stretching sheet, *Pramana*, **95** (2021), 199.
21. A. M. Sedki, Effect of thermal radiation and chemical reaction on mhd mixed convective heat and mass transfer in nanofluid flow due to nonlinear stretching surface through porous medium, *Results Mater.*, **16** (2022), 100334. http://doi.org/10.1016/j.rinma.2022.100334
22. N. Amar, N. Kishan, The influence of radiation on mhd boundary layer flow past a nano fluid wedge embedded in porous media, *Partial Differ. Eq. Appl. Math.*, **4** (2021), 100082.
23. M. V. S. Rao, K. Gangadhar, A. J. Chamkha, Mhd eyring-powell fluid flow over a stratified stretching sheet immersed in a porous medium through mixed convection and viscous dissipation, *Int. J. Modell. Simul.*, **45** (2025), 1640–1656 .
24. T. A. Yusuf, M. B. Ashraf, F. Mabood, Cattaneo–christov heat flux model for three-dimensional magnetohydrodynamic flow of an eyring powell fluid over an exponentially stretching surface with convective boundary condition, *Numer. Methods Partial Differ. Eq.*, **39** (2023), 242–253. http://doi.org/10.18261/pof.39.3.6
25. E. H. Rikitu, Flow dynamics of eyring–powell nanofluid on porous stretching cylinder under magnetic field and viscous dissipation effects, *Adv. Math. Phys.*, **2023** (2023), 9996048.
26. M. Khader, M. Babatin, Numerical study for improvement the cooling process through a model of powell-eyring fluid flow over a stratified stretching sheet with magnetic field, *Case Stud. Therm. Eng.*, **31** (2022), 101786.
27. R. Agrawal, P. Kaswan, Mhd eyring–powell nanofluid past over an unsteady exponentially stretching surface with entropy generation and thermal radiation, *Heat Transfer*, **50** (2021), 4669–4693. http://doi.org/10.1002/htj.22095
28. S. Karthik, D. Iranian, I. Khan, D. B. Basha, F. Hajjej, A. Singh, Heat transfer rate and thermal energy analysis of MHD Powell–Eyring fluid in a permeable medium, *Case Stud. Therm. Eng.*, **52** (2023), 103702.
29. V. S. Patil, A. B. Patil, M. Shamshuddin, P. P. Humane, G. R. Rajput, Eyring–Powell nano liquid flow through permeable elongated sheet conveying inclined magnetic field subject to constructive chemical reaction and multiple slip effects, *Int. J. Modell. Simul.*, **43** (2023), 533–548.
30. H. M. Srivastava, Z. Khan, P. O. Mohammed, E. Al-Sarairah, M. Jawad, R. Jan, Heat transfer of buoyancy and radiation on the free convection boundary layer mhd flow across a stretchable porous sheet, *Energies*, **16** (2022), 58.
31. H. Konwar, Bendangwapang, T. Jamir, Mixed convection mhd boundary layer flow, heat, and mass transfer past an exponential stretching sheet in porous medium with temperature-dependent fluid properties, *Numer. Heat Transfer, Part A: Appl.*, **83** (2023), 1346–1364.

32. W. Abbas, A. M. Megahed, M. Emam, H. M. Sadek, MHD dissipative Powell–Eyring fluid flow due to a stretching sheet with convective boundary conditions and slip velocity, *Sci. Rep.*, **13** (2023), 15674.
33. N. S. Akbar, A. Ebaid, Z. Khan, Numerical analysis of magnetic field effects on eyring-powell fluid flow towards a stretching sheet, *J. Magn. Magn. Mater.*, **382** (2015), 355–358.
34. S. K. Khan, Heat transfer in a viscoelastic fluid flow over a stretching surface with heat source/sink, suction/blowing and radiation, *Int. J. Heat Mass Transfer*, **49** (2006), 628–639.
35. C. Perdikis, A. Raptis, Heat transfer of a micropolar fluid by the presence of radiation, *Heat Mass Transfer*, **31** (1996), 381–382. http://doi.org/10.1007/s002310050071
36. A. Raptis, C. Perdikis, Viscoelastic flow by the presence of radiation, *Z. angew. Math. Mech.* , **78** (1998), 277–279. http://doi.org/10.1002/(SICI)1521-4001(199804)78:4¡277::AID-ZAMM277¿3.0.CO;2-F
37. N. S. Akbar, A. Ebaid, Z. Khan, Numerical analysis of magnetic field effects on Eyring-Powell fluid flow towards a stretching sheet, *J. Magn. Magn. Mater.*, **382** (2015), 355–358.
38. K. Bhattacharyya, S. Mukhopadhyay, G. Layek, Similarity solution of mixed convective boundary layer slip flow over a vertical plate, *Ain Shams Eng. J.*, **4** (2013), 299–305. http://doi.org/10.1016/j.asej.2012.09.003
39. S. Mukhopadhyay, I. C. Mandal, Magnetohydrodynamic (MHD) mixed convection slip flow and heat transfer over a vertical porous plate, *Eng. Sci. Technol. Int. J.*, **18** (2015), 98–105. http://doi.org/10.1365/s35147-015-1272-x
40. M. Fathizadeh, M. Madani, Y. Khan, N. Faraz, A. Yıldırım, S. Tutkun, An effective modification of the homotopy perturbation method for MHD viscous flow over a stretching sheet, *J. King Saud Univ. Sci.*, **25** (2013), 107–113.



AIMS Press